Journal of Photochemistry and Photobiology A: Chemistry 226 (2011) 1–8

Contents lists available at SciVerse ScienceDirect

Journal of Photochemistry and Photobiology A: Chemistry

journal homepage: www.elsevier.com/locate/jphotochem

Photocatalytic activity of TiO_2–SBA-15 under UV and visible light

Hinda Lachheb[a,*], Olfa Ahmed[a], Ammar Houas[a], J.P. Nogier[b]

[a] Equipe de Catalyse et Environnement, URECAP (99/UR/11-20), Ecole Nationale d'Ingénieurs de Gabès/Faculté des Sciences de Gabès, Campus Universitaire, 6072 Gabès, Tunisia
[b] Laboratoire des Systèmes Interfaciaux à l'Echelle Nanométrique (SIEN), UPMC – CNRS UMR 7142, Tour 54 Case Courrier 196, 4 Place Jussieu, Paris 75252 Cedex 05, France

ARTICLE INFO

Article history:
Received 9 June 2011
Received in revised form
10 September 2011
Accepted 18 September 2011
Available online 6 October 2011

Keywords:
TiO_2–SBA-15
Methylene blue
Photocatalysis

ABSTRACT

Supported nanocrystalline titanium dioxide has been prepared by a sol–gel method through the use of mesoporous silica materials SBA-15. The synthesized titania/silica composites were characterized by X-ray diffraction, transmission electron microscopy (TEM) and UV–visible spectroscopy. The TiO_2–SBA-15 composites presented in this study showed much higher photodegradation ability of methylene blue (MB) than commercial pure TiO_2 nanoparticles Degussa P-25 using different light sources (UV, visible and solar light). Experimental results indicate that the photocatalytic activity of titania/silica mixed materials depends on the adsorption ability of composite and the photocatalytic activity of the titania, and the highest activity was observed on the sample with Ti/Si ratio is about 8.

1. Introduction

Titanium dioxide (TiO_2) is one of the most promising semiconductor photocatalysts used for the treatment of waste streams because of its stability under harsh conditions, commercial availability, and excellent semiconductor characteristics. Metal oxide semiconductors, such as TiO_2 and ZnO have been applied as photocatalysts for the removal of highly toxic and non-biodegradable pollutants commonly presented in air and wastewater [1,2]. The efficiency of some commercial TiO_2, especially Degussa P-25, in the treatment of exhaust gas and wastewater contaminated with organic and inorganic pollutants has been fully proved. In order to maximize photoactivity, TiO_2 particles should be small enough to offer a high number of active sites by unit mass [3]. Therefore, in most cases, the samples are ultrafine powders and have large surface area. However, their effective applications are hindered by two serious disadvantages. Firstly, small particles trend to agglomerate into large particles, making against on catalyst performance. Secondly, the separation and recovery of catalyst is difficult [4,5]. For those reasons many researchers have been focused on mesoporous materials supporting titania catalysts.

Considering the mechanism of the heterogeneous photocatalytic reaction, the main drawback of TiO_2 is its relatively low specific surface area (SSA). A great deal of research has been carried out to improve the photocatalytic properties of TiO_2 using a solid support with a primary objective of achieving more active sites per unit area, consequently, a higher photocatalytic reaction rate.

Recently, introducing titanium species into mesoporous silicate materials has attracted much interest because the titanium-containing mesoporous materials have much higher active surface areas (>200 m^2/g) in comparison to pure titania [6], which makes them more effective. Another method of grafting titanium onto mesoporous materials is to modify the inner mesopores with a titanium precursor [7,8]. On this basis, a great effort has been focused in developing supported titania catalysts offering high active surface area and highly dispersed properties.

Up-to-date most of the reported works are mainly based on sol–gel processing using an inert amorphous matrix such as SiO_2 [9–12]. Although this achieved method improved recovery of the catalyst particles, it usually does not allow controlling the particle size. The latter is an important parameter in the titania photocatalytic efficiency as the predominant way of the recombination of electron–hole pairs that may be different depending on the semiconductor particle size range [13]. It is well known that in the nanometer size range, the physical and chemical properties of the semiconductors are modified as compared with bulk semiconductor and strongly affected by the particle size. Small variations in the particle diameters involve great modifications in the surface/bulk ratio thus modifying the significance of volume and surface e^-/h^+ recombination.

In the present work, we have investigated the synthesis of TiO_2–SBA-15 materials by a post-synthesis step via Ti-alkoxide hydrolysis in the support-isopropanol suspension. The samples with different contents of Ti were prepared and followed by heat treatment at 400 °C. The synthesized materials were characterized by various physical techniques. Photocatalytic activity of the samples has been tested using methylene blue as the model pollutant and compared with Degussa P-25.

* Corresponding author. Tel.: +216 75 392600; fax: +216 75 392421.
E-mail address: lachheb2001@yahoo.fr (H. Lachheb).

1010-6030/$ – see front matter © 2011 Elsevier B.V. All rights reserved.
doi:10.1016/j.jphotochem.2011.09.017

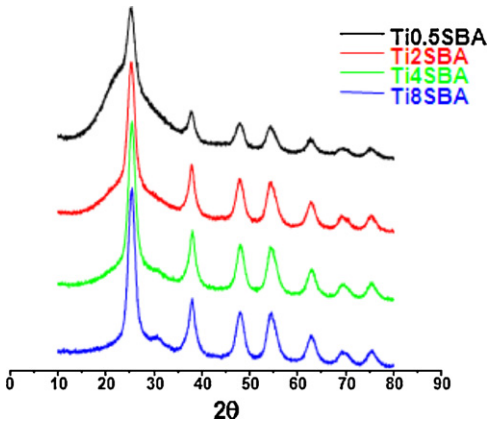

Fig. 1. The wide range XRD patterns of the $(TiO_2)_x$SBA samples calcined at 400 °C.

2. Experimental

2.1. Preparation of Ti-silicate catalysts

The TiO_2–SBA-15 materials were prepared by hydrolysis of titanium tetraisopropoxide sonicated in isopropanol, then the required amount of TTIP was added. A total amount of 8.48 mmol of silica precursor material was added in different molar ratios of Ti/Si, ranging from 0.5 to 8. The resulting mixture was slowly added with water (water/TTIP with volumetric ratio of 160) to cause the hydrolysis of the TTIP. The mixture was centrifuged and the recovered solid was dried at 110 °C over night and calcined at 400 °C for 4 h. The calcination was carried out at 400 °C (2 °C min^{-1}) under oxygen gas for 4 h. The samples will be named by indicating the titania content, support $(TiO_2)_x$SBA-15, where *x* represents the Ti/Si molar ratio.

2.2. Structural characterization of Ti-silicate catalysts

BET surface area, pore volume and average pore diameter of $(TiO_2)_x$SBA-15 photocatalysts were measured by N_2 physisorption at 77 K using Micrometrics ASAP 2020 system. Powder XRD patterns of the catalyst samples were determined on a XD-2 powder X-ray diffractometer using CuKα radiation of wavelength 0.154 nm over the scan range $2\theta = 10–80°$ for wide angle XRD. Crystallite diameter ($D_{anatase}$) of $(TiO_2)_x$SBA-15 was determined from the broadening (peak width at half maximum minus instrumental broadening) of the anatase main peak at $2\theta = 25°$ size using Scherrer's formula $D_{anatase} = 0.91\lambda/\beta\cos\theta$.

2.3. Photocatalytic reactions

The photodegradation of MB was performed in order to evaluate the photocatalytic activity of prepared titania/silica materials. The experiments were carried out in a Pyrex batch reactor with cylindrical shape containing 125 mL of MB solution with an initial concentration of 30 mg/L at natural pH and at room temperature to assure the adsorption equilibrium was reached. The light source used with UV-irradiation was provided by a high pressure mercury lamp (Philips HPK-125W, $\lambda_{max} = 365$ nm) and visible halogen lamps (60, 150 and 250 W) with a wavelength of 650 nm immersed within the reactor in a double wall jacket. The methylene blue degradation reaction have been transposed to the solar light and used to determine the efficiency of $(TiO_2)_x$SBA using solar energy. Commercial pure TiO_2 nanoparticles (Degussa P-25) 0.5 g/L were used for this experiment and the amount of TiO_2/SiO_2 materials necessary to achieve the same TiO_2 loading. The comparison of tested catalysts was done at this fixed TiO_2 concentrations because in our experimental conditions, only the semiconductor particles were expected to show photocatalytic activity. Before analysis, the aqueous samples were filtered through a 0.45 μm membrane filter to remove TiO_2 agglomerates in suspension. A Schimadzu-1700 UV-Vis spectrophotometer was used to determine the concentration of the MB and to follow their kinetic disappearance. Calibration plots based on Beer–Lambert's law were established to relate the absorbance to the concentration. The molar extinction coefficient for MB was 71.105 L/(mol cm) estimated at 665 nm. Suspension samples of 5 mL volume were collected at fixed time intervals, filtered and the concentration of MB was determined by UV-visible spectrophotometer.

3. Results and discussion

3.1. XRD

Fig. 1 shows the XRD patterns of TiO_2 supported on SBA-15 with TiO_2 content range of 0.5–8 molar ratio. Along with the decrease in titania content, the (1 0 1) reflection due to anatase was found to increase. The XRD patterns at higher angles of the supported TiO_2 samples evidenced that anatase was the only titania phase present in all prepared samples calcined at 400° as indicated by the peak emerging at 25.4° associated with (1 0 1) anatase diffraction. No rutile phase was detected in any case according to the absence of (1 1 0) rutile reflection at 27.4°. The XRD patterns of $(TiO_2)_{0.5}$SBA-15 is very similar to those reported by other studies, indicating that the broad XRD reflection peak at 23° is caused by the very small size of the solid [14,15]. Also, Fig. 1 shows that the highest peak for $(TiO_2)_x$SBA-15 is closed to 2θ equal to 25°, which is similar to that observed for anatase. In contrast, rutile has its highest peak at about 2θ equal to 54° or 56°. Therefore, it can be expected that all the samples have properties that are similar to those of anatase. The results show that the $D_{anatase}$ increase with increasing TiO_2 content (Table 1). No rutile formation was observed in $(TiO_2)_8$SBA calcined up to 700 °C(Table 4). Thermal stability of the anatase crystalline phase is probably due to a stabilizing effect of silica on the anatase-rutile transition at higher temperatures [16,17].

3.2. N_2 adsorption–desorption isotherms

Fig. 2 shows N_2 adsorption isotherms from calcined samples with varying titanium loadings. All materials give typical irreversible type IV adsorption isotherms with a H1 hysteresis loop as defined by IUPAC [18]. N_2 adsorption at low relative pressure ($P/P_0 < 0.3$) is accounted for by monolayer adsorption of N_2 on the

Table 1
Textural properties of supports and prepared samples.

Catalyst	Structure	$D_{anatase}$ (nm)	SSA (m^2/g)	V_{pore} (mL/g)	d_{pore} (nm)
$(TiO_2)_0$SBA	–	–	574	1.03	7.2
$(TiO_2)_{0.5}$SBA	Anatase	4.43	400	1.10	6.8
$(TiO_2)_2$SBA	Anatase	4.52	340	1.30	6.5
$(TiO_2)_4$SBA	Anatase	4.70	300	1.30	6.5
$(TiO_2)_8$SBA	Anatase	5.20	200	1.30	6.3
Degussa P25	Anatase/rutile	–	50	–	–

Table 2
Adsorption characteristics of MB.

Catalysts	q_{max} (mg/g)	K_{ads} (L/mg)
$(TiO_2)_0$SBA	55.00	3.00
$(TiO_2)_{0.5}$SBA	47.60	2.30
$(TiO_2)_2$SBA	39.56	0.80
$(TiO_2)_4$SBA	34.12	0.36
$(TiO_2)_8$SBA	25.00	0.09
Degussa P25	20.32	0.03

pore walls and does not indicate the presence of micropores. The calculated BET or specific surface area of $(TiO_2)_0$SBA-15 is around 574.0 m^2/g. This value becomes smaller after the grafting of titanium species on the pores walls of SBA-15, as indicated in Table 1. The reduction in size is especially reflected in the BET surface area, which showed a reduction of about 65% $(TiO_2)_8$SBA-15. The observation of the decreased surface area may be an indication of the formation of TiO_2 clusters within the mesopores. The values of SSA, V_{pore} and d_{pore} are summarized in Table 1. The results show that the TiO_2 content clearly affects SSA and pore characteristics of Ti-silicates. For $(TiO_2)_8$SBA, the BET surface area, d_{pore} and pore volumes decrease with the increase of calcination temperature (Table 4).

3.3. Diffuse reflective UV–visible spectroscopy

DRS spectra are shown in Fig. 3. For low titanium loading samples ($(TiO_2)_{0.5}$SBA), the observed absorption maximum band is at 290 nm. For increasing titanium loading, this maximum band shifts to near 300 nm ($(TiO_2)_8$SBA). Its intensity increases with increasing titanium content. The absorption edge shifts towards shorter wavelengths for the TiO_2/SBA-15 sample and clearly indicates an increase in the band gap of as-synthesized TiO_2 particles inside the SBA-15. Band gap energy can be estimated from a plot of $(\alpha)^{1/2}$ versus photon energy ($h\upsilon$) (Fig. 4). The intercept of the tangent to the plot direct gives a good approximation of the band gap energy for indirect band gap materials such as TiO_2 [19,20]. The larger varied between 3.3 and 3.6 eV respectively $(TiO_2)_{0.5}$SBA and $(TiO_2)_8$SBA. The larger band gap of the TiO_2 nanocrystals can be attributed to the quantum size effect. This is because the as-prepared TiO_2 nanoparticles have smaller crystalline size limited by SBA-15 nanometer channels [21]. This result strongly suggests that the addition of SBA-15 can effectively suppress the growth of TiO_2 particles (Table 1).

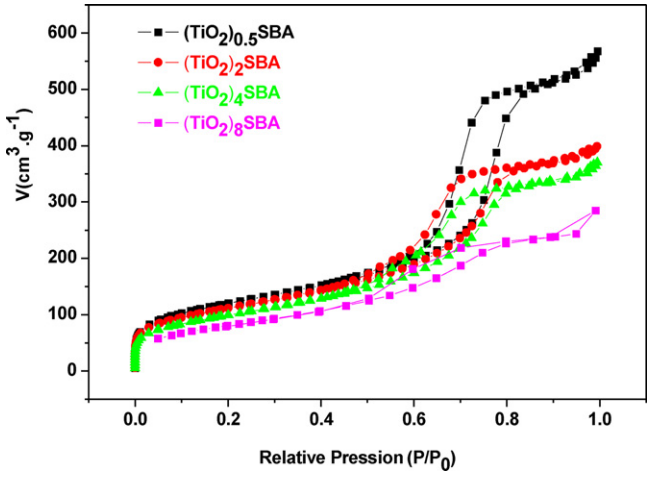

Fig. 2. N_2 adsorption–desorption isotherms of $(TiO_2)_x$SBA calcined at 400 °C.

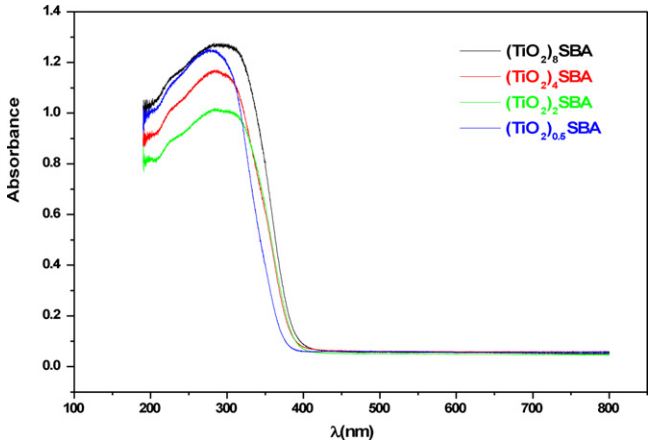

Fig. 3. UV–vis absorption spectra of the $(TiO_2)_x$SBA samples.

3.4. TEM

The transmission electron microscope lattice image of $(TiO_2)_x$SBA (x = 0, 0.5, 2 and 4) samples are shown in Fig. 5. It shows that the highly ordered pore structure of pure SBA-15 described in literature [22,23] with a pore diameter of 7 nm is well recognized in Fig. 5A. Moreover, the regular silica morphology is at least partially maintained in Ti-silicates up to TiO_2 content of 0.5. Increasing the TiO_2 content up to $(TiO_2)_4$SBA, however, destroys the ordered silica pore arrangement completely (Fig. 5D). TEM pictures of $(TiO_2)_x$SBA-15 display some small dark spots on the silica framework (Fig. 5C and D) since these structures are not present in pure SBA-15 (Fig. 5A), they are probably associated with the presence of TiO_2. The localization of TiO_2 on the external silica surface is further supported by the negligible effect of TiO_2 content on V_{pore} and d_{pore} (Table 1). Decreased SSA probably is a result of the loss of ordered pore arrangement, as observed by TEM (Fig. 5A–D) and XRD (Fig. 1).

3.5. Photocatalytic activity

3.5.1. UV-light

Methylene blue photodegradation test reactions were carried out in order to evaluate the activity of the prepared catalysts. In photodegradation experiments, there are two factors resulting in the decreasing of the concentration of MB: the adsorption of the MB onto the surface of the photocatalyst and the photodegradation of MB. The kinetics of adsorption for MB (30 ppm) are represented in

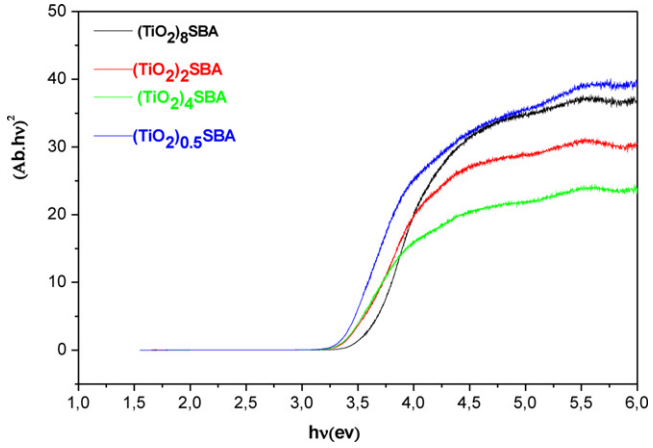

Fig. 4. Plots of $\alpha^{1/2}$ versus photon energy ($h\upsilon$) for $(TiO_2)_x$SBA.

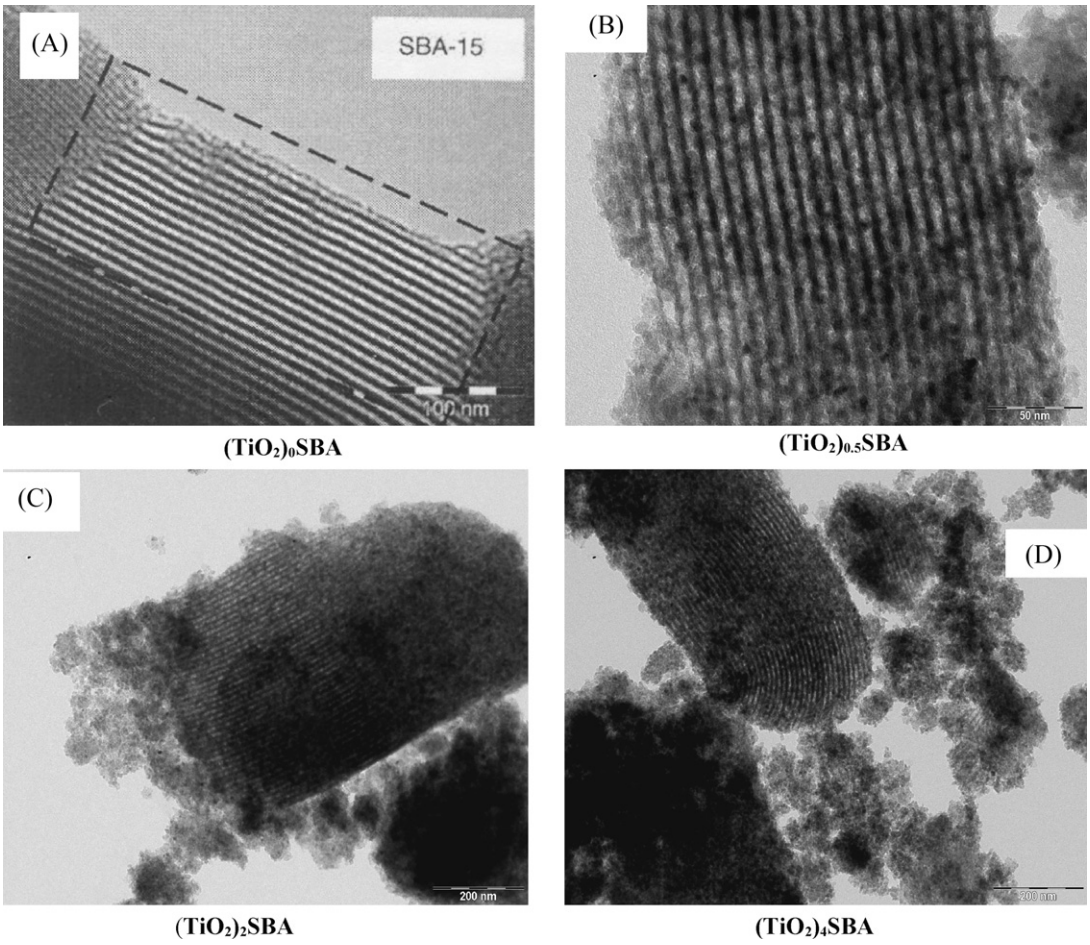

Fig. 5. TEM image of $(TiO_2)_0$SBA (A), $(TiO_2)_{0.5}$SBA (B), $(TiO_2)_2$SBA (C) and $(TiO_2)_4$SBA (D).

Fig. 6 in the presence of $(TiO_2)_x$SBA samples with different contents of TiO_2 (x = 0.5, 2, 4 and 8) and commercial Degussa P-25. It can be observed that the steady state of adsorption is reached within 1 h. Therefore, this time has been selected for the initial period in the dark previously to UV-irradiation at time t_{UV} = 0 min to make sure that initial degradation initiates at the equilibrium of adsorption. The maximum adsorbed quantities q_{max} and the adsorption constants K_{ads} of MB were determined at different initial concentrations varying between 5 and 30 mg/L using the linear transform of the Langmuir equation.

$$\frac{C_e}{q_e} = \frac{1}{kq_{max}} + \frac{C_e}{q_{max}}$$

where C_e is the equilibrium concentration of the dye and q_e is the quantity of the adsorbed MB at the photocatalyst surface. The linearity of the curves clearly indicates that the Langmuir isotherm is correctly observed, implying a monolayer adsorption model. The calculated values are listed in Table 2. The adsorption constants K_{ads} vary from 0.03 to 3.0 L/mg. The incorporation ratio of titanium that resulted in the highest maximum adsorption capacities was $(TiO_2)_{0.5}$SBA. MB sorption capacity decreased when the molar ratio increased from 0.5 to 8 (Fig. 7), possibly due to incorporation of Ti into the silica framework. Ti that the silica framework would not

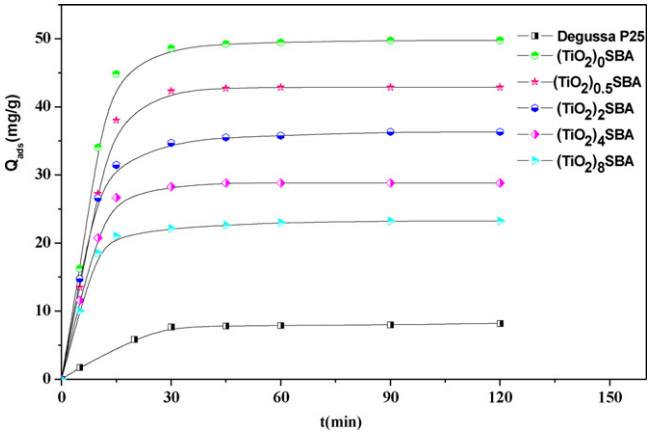

Fig. 6. Kinetics of adsorption of MB adsorption in the presence of $(TiO_2)_x$SBA and Degussa P-25. Conditions: C_0 = 30 ppm, m(catalyst) = 62.5 mg, V = 125 mL, natural pH, T = 30 °C.

Table 3
Rate constant of $(TiO_2)_x$SBA-15 and Degussa P25 for MB photodegradation.

Catalysts	Content of titania (g)	k_{app}(min^{-1})		
		UV light	Visible light (250 W)	Solar light
$(TiO_2)_0$SBA	0.00	0.012	0.008	0.005
$(TiO_2)_{0.5}$SBA	0.57	0.027	0.011	0.009
$(TiO_2)_2$SBA	2.34	0.048	0.021	0.018
$(TiO_2)_4$SBA	4.75	0.090	0.041	0.034
$(TiO_2)_8$SBA	9.96	0.130	0.075	0.064
Degussa P25	–	0.116	0.055	0.033

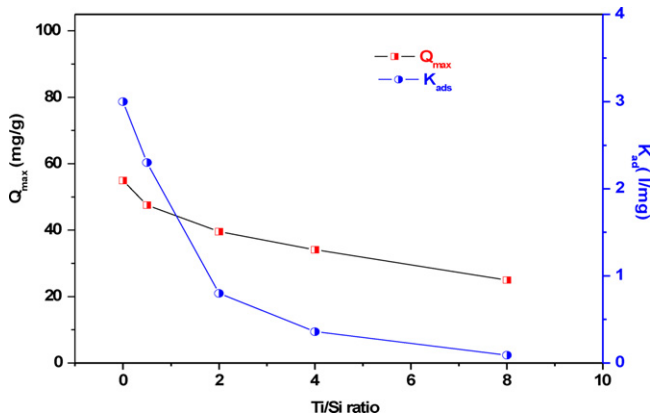

Fig. 7. Linear variations between the (Q_{max}, K_{ads}) of adsorbed MB and the Ti/Si ratio.

function as reactive sorption sites for MB removal. Similar results have been observed in other studies that investigated La_xSBA-15, Al_xSBA-15, and Fe_xSBA-15 [24].

The following general observations can be made. For both unsupported Degussa P-25 and $(TiO_2)_x$SBA photocatalysts, the maximum quantities of adsorbed MB increase in the following order:

$$\text{P-25} < (TiO_2)_8\text{SBA} < (TiO_2)_4\text{SBA} < (TiO_2)_2\text{SBA} < (TiO_2)_{0.5}\text{SBA} < (TiO_2)_0\text{SBA}$$

The $(TiO_2)_x$SBA samples exhibits a much higher adsorption capability of MB than Degussa P-25, which is attributed to their much higher specific surface area and pore volumes than pure Degussa P-25 [12].

Fig. 8 shows the degradation curves of MB with UV light by $(TiO_2)_x$SBA samples with different contents of TiO_2 and commercial Degussa P-25, without UV irradiation, during the initial 90 min the concentration of MB rapidly decreased and 60% is discolored, which was due to the adsorption of dye on catalyst surface. The adsorption amount of MB on $(TiO_2)_x$SBA (adsorption capacity of 60% in the presence of $(TiO_2)_8$SBA) is much higher than that Degussa P-25 (20%), because these catalysts have larger surface area and pore volume (Table 1).

Blank experiments were also carried out in the presence of SBA-15, no obvious photodegradation was observed, all the samples show photocatalytic activity, and the MB conversion depends on the Ti content in the TiO_2–SBA materials. The MB was

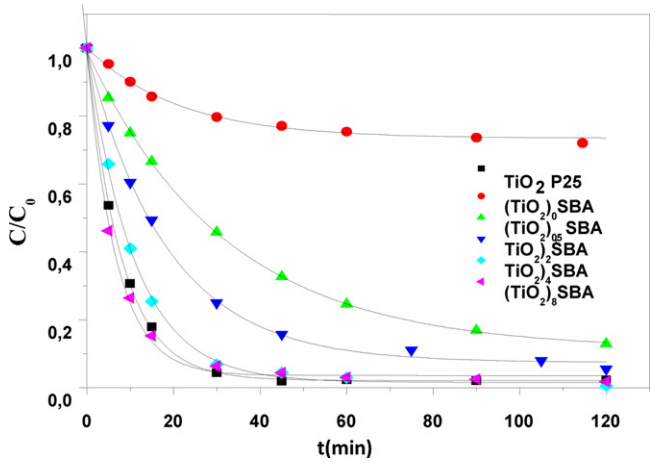

Fig. 8. The photocatalytic performance of the $(TiO_2)_x$SBA-15 samples and Degussa P-25. Conditions: C_0 = 30 ppm, m(catalyst) = 62.5 mg, V = 125 mL, natural pH, T = 30 °C.

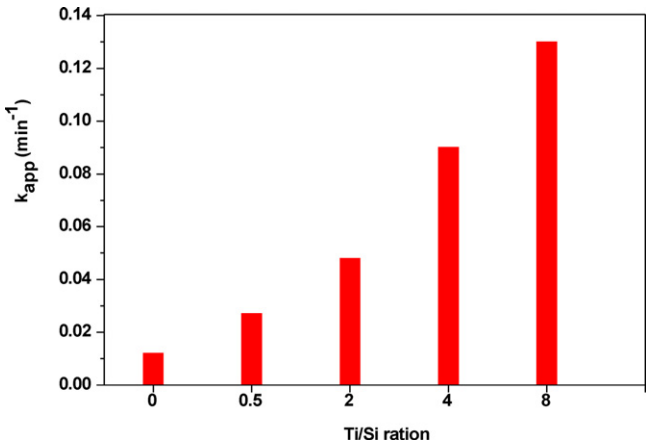

Fig. 9. Effect of the Ti/Si ration on the degradation of methylene blue. Conditions: C_0 = 30 ppm, m(catalyst) = 62.5 mg, V = 125 mL, natural pH, T = 30 °C.

photocatalytic decomposed by TiO_2–SBA at higher Ti loading which demonstrated that Ti in the silica is also active for photocatalytic reaction. We can seen that besides the adsorption ability of catalysts, other factors, such as crystal phase, surface area, crystalline size and crystallinity, also play an important role in influencing photoactivity.

The apparent rate constants of different photocatalysts were calculated (Fig. 9) and listed in Table 3. It can be clearly seen that the addition of titania is necessary for photocatalytic activity, significantly improve the photodegradation activity of the catalysts. Catalyst $(TiO_2)_8$SBA has the highest rate constant of 0.13 min^{-1}, which is higher than that of Degussa P-25 (0.116 min^{-1}), whereas, $(TiO_2)_0$SBA has the lowest rate constant of 0.012 min^{-1}. It is generally accepted that for effective degradation, the organic materials should be concentrated at the TiO_2 surface firstly, and the large surface area of $(TiO_2)_x$SBA samples also can adsorb significant amounts of water and hydroxyl groups, which react with photoexcited holes on the catalyst surface and can produce hydroxyl radicals [25]. Interesting, the removal rate of MB increased when the molar ratio of ($(TiO_2)_x$SBA) increased from 0.5 to 8. This is due to the fact that titanium is well dispersed in the synthesized samples. In addition, according to Zhang et al. [3], the photocatalytic activity depends on the titania mean particle size since the nanocrystalline TiO_2 will influence the dynamic of e^-/h^+ recombination.

Authors showed that it was reported that the rates of photodecomposition of MB using TiO_2 photocatalyst were enhanced by loading TiO_2 particles onto adsorption such as silica. Using mixed SiO_2 and TiO_2 resulted in enhanced photocatalytic efficiencies in the destruction of other dyes (Orange G [26], rhodamine-6G [27] and ethylene [28]) compared with Degussa P25 alone. The beneficial effect of SiO_2, which shows no photoactivity, probably relates the preferential adsorption of the substrates on SiO_2. And Chen et al. [29] suggested that the doping of SiO_2 has no effect on the crystal structure and the surface groups of TiO_2, except for increasing the specific surface area.

0.5 g/L $(TiO_2)_8$SBA catalyst was reused three times under UV light to degrade 30 mg/L of methylene blue, washing the catalyst with water after each use, putting a new quantity of MB, and repeating the repetitive experiments. The results were similar as shown in Fig. 10, but the degradation efficiency was decreased slightly from 0.922 to 0.859 after 60 min degradation. Such repetitive experiments also proved that $(TiO_2)_8$SBA was stable photocatalyst, and not decompose after under UV-light.

Fig. 11 shows the degradation of MB by $(TiO_2)_8$SBA calcined at different temperatures, an increase of the dye decomposition with increasing calcination temperature was observed. The

Table 4
Textural properties of $(TiO_2)_8$SBA samples calcined at different temperatures.

Catalyst	Structure	$D_{anatase}$ (nm)	SSA (m^2/g)	V_{pore} (mL/g)	d_{pore} (nm)
$(TiO_2)_8$SBA-400	Anatase	5.2	200	1.30	6.3
$(TiO_2)_8$SBA-550	Anatase	5.8	155	1.10	6.1
$(TiO_2)_8$SBA -700	Anatase	6.2	105	0.90	5.2

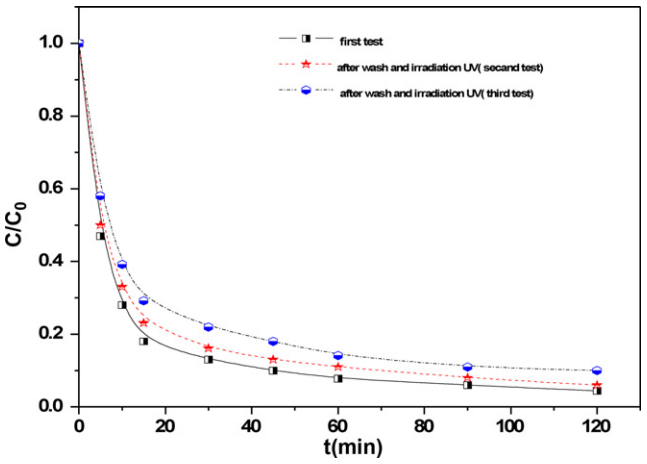

Fig. 10. The influence of the reuse of $(TiO_2)_8$SBA-15 catalyst on the degradation efficiency. Conditions: C_0 = 30 ppm, m(catalyst) = 62.5 mg, V = 125 mL, natural pH, T = 30 °C.

photocatalytic activities of TiO_2/SBA samples decreased as the following order: 700 °C > 550 °C > 400 °C. It confirms that $(TiO_2)_8$SBA-700 has more photocatalytic effect on the degradation of MB than other catalyst could be explained by their phase composition [30]. It is clear that there are several factors such as crystal phase, surface area, crystalline size, and more accessible photo-oxidative sites [30] can play an important role in influencing photoactivity. Though the sample calcined at 400 °C has the highest BET surface area and smaller particle size but its crystallinity is worse than those calcined at higher temperature leading to law photoactivity.

3.5.2. Visible light

In the presence of visible light at 250 W intensity, $(TiO_2)_8$SBA was compared to that of TiO_2 P-25 catalyst, in all cases the

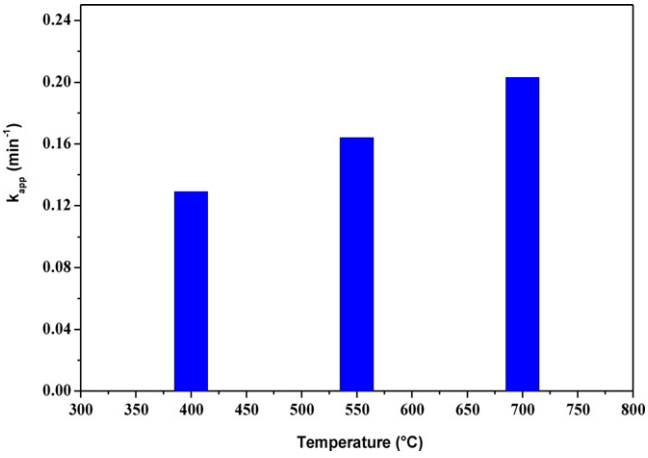

Fig. 11. The photocatalytic activity of $(TiO_2)_8$SBA samples calcined at different temperatures. Conditions: C_0 = 30 ppm, m(catalyst) = 62.5 mg, V = 125 mL, natural pH, T = 30 °C.

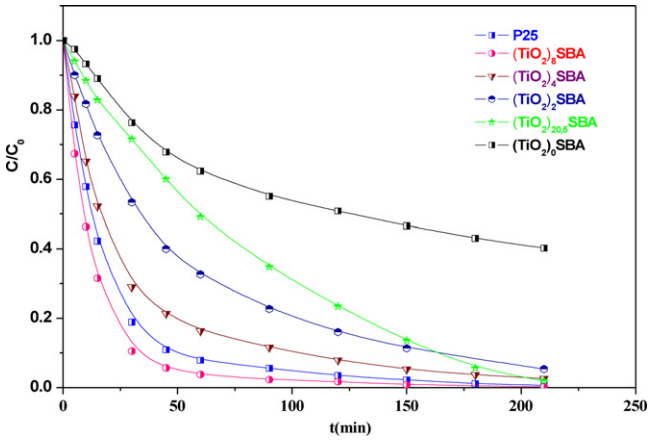

Fig. 12. Photocatalytic MB degradation under visible light of $(TiO_2)_x$SBA and Degussa P-25. Conditions: C_0 = 30 ppm, m(catalyst) = 62.5 mg, V = 125 mL, natural pH, T = 30 °C.

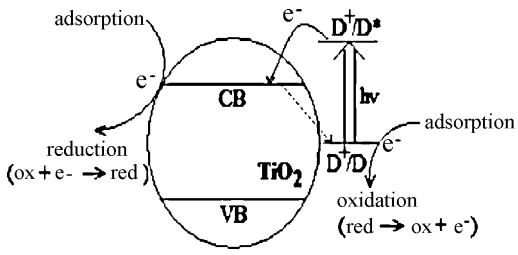

Scheme 1. Photosensitized degradation reaction on sensitized TiO_2 particle (λ > 400 nm).

results showed photocatalytic efficiency decomposition of MB in the presence of $(TiO_2)_8$SBA than Degussa P-25 using visible light irradiation (Fig. 12). Blank experiments were carried out in the presence of SBA-15, no photodegradation of MB was observed.

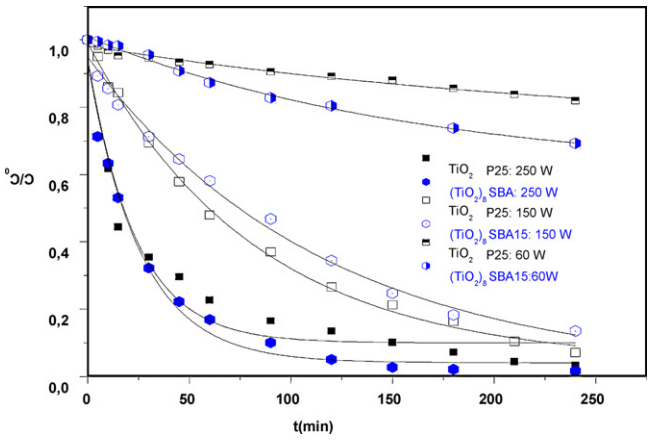

Fig. 13. Photocatalytic MB degradation under visible light at different intensities (60, 150 and 250 W) of $(TiO_2)_8$SBA and Degussa P-25. Conditions: C_0 = 30 ppm, m(catalyst) = 62.5 mg, V = 125 mL, natural pH, T = 30 °C.

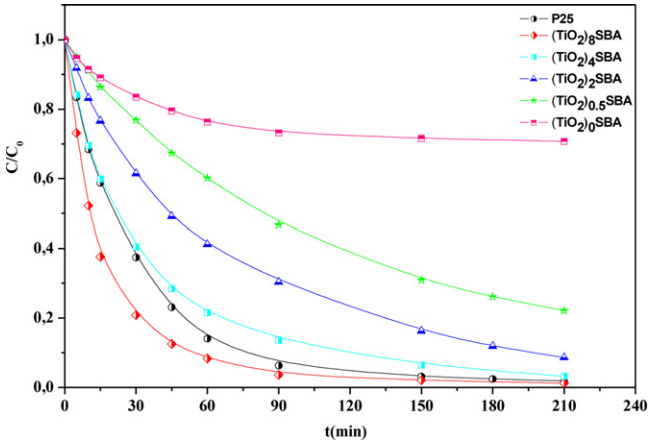

Fig. 14. Photocatalytic MB degradation under solar light of $(TiO_2)_x$SBA and Degussa P-25. Conditions: C_0 = 30 ppm, m(catalyst) = 62.5 mg, V = 125 mL, natural pH, T = 30 °C.

Our results confirm that $(TiO_2)_8$SBA has more photocatalytic effect on the degradation of the dye than Degussa P-25, and a complete decoloration is observed within 4 h. It is well known that titania is photoinactive under visible light, the process of the photobleaching has to involve the dye as a sensitizer. Other results have shown the photocatalytic efficiency of dye-sensitized TiO_2–SBA on visible light illumination [23]. The photosensitization process can expand the wavelength range of excitation for the photocatalyst through excitation of the dye molecules followed by charge transfer to TiO_2 (Scheme 1). The organic dye serves as both a sensitizer and a substrate to be degraded [31–35,27,36–40].

When D stands for sensitizer, D* is the electronically excited sensitizer and D^+ is the oxidized sensitizer. The mechanism of photocatalytic decomposition of azo dyes has been widely discussed. The vis/TiO_2 photocatalysis of the dye involves the following reactions [41]:

$$D + h\nu(\text{visible}) \rightarrow D*$$

$$D^* + TiO_2 \rightarrow D^{*+} + e^-_{TiO_2}$$

$$e^-_{TiO_2} + O_2 \rightarrow TiO_2 + O_2^{\bullet -}$$

At different intensities (60, 150 and 250 W), the results illustrated in Fig. 13 showed the proportional linear dependence between the decomposition rates of MB and the intensity of the lamp. The curves indicate the efficiency of $(TiO_2)_8$SBA irradiated with 250 W, when a total degradation of MB observed after 4 h illumination.

3.5.3. Solar light

The solar experiments are shown in Fig. 14, from these results, it can be seen that the photocatalytic degradation of MB in the presence of $(TiO_2)_x$SBA is important, in particular, even though all methylene blue has disappeared. The photodegradation of MB was performed using TiO_2 supported on silica. In the presence of $(TiO_2)_8$SBA, the curves show that after 2 h of the phototreatment, 95% of the dye was eliminated. The results also indicate the slight benefits that were achieved by adding $(TiO_2)_8$SBA compared with the Degussa P-25. The calculated rate constant of different photocatalysts irradiated with different intensities (UV, Vis and solar light) are listed in Table 3, in all cases, the highest oxidation of organic pollutant is observed in the presence of $(TiO_2)_8$SBA.

4. Conclusion

The titania containing SBA-15 is prepared by the direct synthesis method with varying titanium loadings and the photocatalytic activity of synthesized TiO_2–SBA-15 materials is tested by decomposition of MB. A combination of XRD, nitrogen adsorption–desorption isotherm, TEM as well as solid state UV–visible spectroscopy has been used to characterize the titania modified SBA-15 materials. These characterization methods allowed the evaluation of the assembling modes of TiO_2 inside SBA-15. The application of the catalyst supported on silica creates opportunity to reduce the time of dye decolorisation. In all cases, the degradation of MB increased with increasing the TiO_2 content. Results show an enhanced photocatalytic efficiency of decomposing MB in the presence of $(TiO_2)_8$SBA under visible and solar light irradiation. A total decolorisation was observed in a short time, this indicates that is possible to develop the high photocatalytic materials with dye-sensitized TiO_2 immobilized inside SBA-15 pores, in combination of the high specific surface area of SBA-15 and high photocatalytic efficiency of dye-sensitized TiO_2 on visible light illumination.

Acknowledgements

Special thanks to the Tunisian and French governments: Cooperation Tuniso-Française: Recherche Scientifique et Technologique (CMCU) for mission Financial support.

References

[1] M.A. Fox, M. Dulay, Heterogeneous photocatalysis, Chem. Rev. 93 (1993).
[2] M.R. Hoffmann, S.T. Martin, W.Y. Choi, D.W. Bahnemann, Environmental applications of semiconductor photocatalysis, Chem. Rev. 95 (1995) 69.
[3] Z. Zhang, C.C. Wang, R. Zakaria, J.Y. Ying, Role of particle size in nanocrystalline TiO_2-photocatalysts, J. Phys. Chem. B 102 (1998) 10871.
[4] Y. Zhu, L. Zhang, W. Yao, L. Cao, The chemical states and properties of doped TiO_2 film photocatalyst prepared using the sol–gel method with $TiCl_4$ as a precursor, Appl. Surf. Sci. 158 (2000) 32.
[5] J.C. Yu, J.G. Yu, J.C. Zhao, Enhanced photocatalytic activity of mesoporous and ordinary TiO_2 thin film by sulfuric acid treatment, Appl. Catal. B: Environ. 36 (2002) 31.
[6] T. Maschmeyer, F. Rey, G. Sanker, J.M. Thomas, Nature (London) 378 (1997) 159.
[7] B.J. Aronson, C.F. Blanford, A. Stein, Chem. Mater. 9 (1997) 2842.
[8] Z. Luan, W.M. Macs, P.A.W. vander Heide, D. Zhao, R.S. Czernuszewicz, L. Kevan, Chem. Mater. 11 (1999) 3680.
[9] K. De Witte, A.M. Busuioc, V. Meynen, M. Mertens, N. Bilba, G. Van Tendeloo, P. Cool, E.F. Vansant, Micropor. Mesopor. Mater. 110 (1) (2008) 100–110.
[10] A.M. Busuioc, V. Meynen, E. Beyers, M. Mertens, P. Cool, N. Bilba, E.F. Vansant, Appl. Catal. A: Gen. 312 (2006) 153.
[11] D.R. Sahu, L.Y. Hong, S.-C. Wang, J.-L. Huang, Micropor. Mesopor. Mater. 117 (3) (2009) 640–649.
[12] J. Yang, J. Zhang, L. Zhu, S. Chen, Y. Zhang, Y. Tang, Y. Zhu, Y. Li, J. Hazard. Mater. 137 (2) (2006) 952–958.
[13] N. Serpone, D. Lawless, R. Khairtudinov, E. Pelizzetti, J. Phys. Chem. 99 (1995) 16655.
[14] B.L. Newalkar, J. Olanrewaju, S. Komarneni, Application of large pore MCM-41 molecular sieves to improve pore size analysis using nitrogen adsorption measurements, Langmuir 13 (2001) 6267–6273.
[15] W. Wang, M. Song, Photocatalytic activity of titania-containing mesoporous SBA-15 silica, Micropor. Mesopor. Mater. 96 (2006) 255–261.
[16] K.Y. Jung, S.B. Park, J. Photochem. Photobiol. A: Chem. 127 (1999) 117–122.
[17] R. van Grieken, J. Aguado, M.J. Lopez-Munoz, J. Marugan, J. Photochem. Photobiol. A 148 (2002) 315–322.
[18] K.S.W. Sing, D.H. Everett, R.A.W. Haul, L. Moscow, R.A. Pierotti, J. Rouquerol, T. Siemieniewska, Pure Appl. Chem. 57 (1985) 603.
[19] M.M. Bahnemann, K.M. Krishna, T. Soga, T. Jimbo, M. Umeno, J. Chem. Solids 60 (1999) 201.
[20] C. Kormann, D.W. Bahnemann, M.R. Hoffmann, J. Phys. Chem. 92 (1988) 5196.
[21] F. Gao, Q.Y. Lu, D.Y. Zhao, Chem. Phys. Lett. 360 (2002) 585.
[22] D. Zhao, J. Feng, Q. Huo, N. Melosh, G.H. Fredrickson, B.F. Chmelka, G.D. Stucky, Science 279 (1998) 548–552.
[23] H. ding, H. Sun, Y. Shan, J. Photochem. Photobiol. A: Chem. 169 (2005) 101–107.
[24] M. Jang, J.K. Park, E.W. Shin, Micropor. Mesopor. Mater. 75 (2004) 159–168.
[25] C.S. Turchi, D.F. Ollis, Photocatalytic degradation of organic-water contaminants mechanisms involving hydroxyl radical attack, J. Catal. 122 (1990) 178.
[26] G. Li, X.S. Zhao, Ind. Eng. Chem. Res. 45 (2006) 3569–3573.
[27] C. Anderson, A.J. Bard, J. Phys. Chem. 99 (1995) 9882.

[28] X. Fu, L.A. Clark, Q. Yang, M.A. Anderson, Environ. Sci. Technol. 30 (1996) 647.
[29] Z. Chen, G. Yu, P. Zhang, Z. Jiang, Huan Jing Ke Xue 23 (2002) 40–44.
[30] S. Zhu, Di. Zhang, X. Zhang, L. Zhang, X. Ma, Y. Zhang, M. Cai, Micropor. Mesopor. Mater. (2009).
[31] A.L. Linsebigler, G. Lu, J.T. Yates Jr., Chem. Rev. 95 (1995) 735.
[32] K. Vinodgopal, P.V. Kamat, J. Phys. Chem. 96 (1992) 5053.
[33] K. Vinodgopal, P.V. Kamat, Environ. Sci. Technol. 26 (1992) 1963–1966.
[34] A. Mills, A. Belghazi, R.H. Davies, D. Worsley, S. Morris, J. Photochem. Photobiol. A: Chem. 79 (1994) 131.
[35] H. Ross, J. Bindig, S. Hecht, Sol. Energy Mater. Sol. Cells 33 (1994) 475.
[36] K. Vinodgopal, D.E. Wynkoop, P.V. Kamat, Environ. Sci. Technol. 30 (1996) 1660.
[37] C. Nasr, K. Vinodopal, L. Fisher, S. Hotchandani, A.K. Chattopadhyay, P.V. Kamat, J. Phys. Chem. 100 (1996) 8436.
[38] J. Lobedank, E. Bellmann, J. Bendig, J. Photochem. Photobiol. A: Chem. 108 (1997) 89.
[39] F. Zhang, J. Zhao, L. Zang, T. Shen, H. Hidaka, E. Pelizzetti, N. Serpone, J. Mol. Catal. A: Chem. 120 (1997) 173.
[40] K. Kalyanasundaram, M. Graetzel, Coord. Chem. Rev. 77 (1998) 347.
[41] C. Galindo, P. Jacques, A. Kalt, Chemosphere 45 (2001) 997.